

LMI-based robust model predictive control for a quarter car with series active variable geometry suspension

Zilin Feng, Anastasis Georgiou, Simos A. Evangelou, Min Yu, Imad M Jaimoukha and Daniele Dini

Abstract—This paper proposes a robust model predictive control-based solution for the recently introduced series active variable geometry suspension (SAVGS) to improve the ride comfort and road holding of a quarter car. In order to close the gap between the nonlinear multi-body SAVGS model and its linear equivalent, a new uncertain system characterization is proposed that captures unmodeled dynamics, parameter variation, and external disturbances. Based on the newly proposed linear uncertain model for the quarter car SAVGS system, a constrained optimal control problem (OCP) is presented in the form of a linear matrix inequality (LMI) optimization. More specifically, utilizing semidefinite relaxation techniques a state-feedback robust model predictive control (RMPC) scheme is presented and integrated with the nonlinear multi-body SAVGS model, where state-feedback gain and control perturbation are computed online to optimise performance, while physical and design constraints are preserved. Numerical simulation results with different ISO-defined road events demonstrate the robustness and significant performance improvement in terms of ride comfort and road holding of the proposed approach, as compared to the conventional passive suspension, as well as, to actively controlled SAVGS by a previously developed conventional H_∞ control scheme.

Index Terms—Active suspension, Quarter car geometry, RMPC, Robust control application, Uncertain Systems.

I. INTRODUCTION

The suspension system refers to the entire support system composed of springs and shock absorbers between the vehicle body and wheels. The function of the suspension system is to isolate passengers from vibration and shocks induced by road disturbances to improve ride comfort while providing good road holding [1]. The passive suspension includes a conventional spring-damper unit, which passively adapts to the road profile and dissipates energy from road perturbations. Active suspension systems have become widely available and popular since the 1980s. With improved ride comfort as compared to passive suspension, concise structure, reduced energy costs and high reliability, they are continuously pursued in the process of vehicle and transportation electrification.

Recently, a novel mechatronic suspension solution, the Series Active Variable Geometry Suspension (SAVGS), has been conceptualised, designed, optimised, and experimentally validated through both quarter-car prototyping and full-car road testing [2]–[8]. Fig. 1 shows the SAVGS application to

a quarter-car with a double-wishbone suspension, where the active single-link component (‘F-G’) is introduced between the chassis (‘G’) and the upper-end eye of the spring damper unit (‘F’), in series with the conventional spring-damper. The single-link (SL) is driven by a rotary permanent magnet synchronous motor (PMSM) actuator, which generates the torque (T_{SL}) acting from the chassis onto the lower wishbone (through the spring-damper) to improve the performance of a double-wishbone suspension. As compared with other active suspensions, the SAVGS features [2]: i) potential for improvement of ride comfort and road holding, ii) negligible unsprung mass and small sprung mass increment, iii) low power actuation requirements, and iv) fail-safe characteristics.

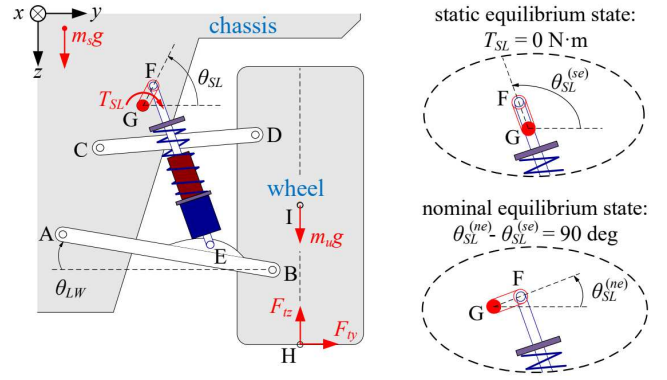


Fig. 1. SAVGS application to a quarter car double-wishbone suspension [4]. θ_{SL} denotes the single-link angle with respect to the horizontal plane (as shown in the diagram it has a negative value). The superscript (*se*) refers to the static equilibrium state with zero torque $T_{SL} = 0$ applied on the single link. The superscript (*ne*) denotes the nominal equilibrium state, where $\theta_{SL}^{(ne)} - \theta_{SL}^{(se)} = \Delta\theta_{SL}^{(ne)} = 90^\circ$ (Note that $\theta_{SL} - \theta_{SL}^{(se)} = \Delta\theta_{SL}$).

Previous works have employed robust control methodologies for the ride comfort and road-holding enhancement of automobile active suspension systems and achieved reasonable success. For example, the H_∞ control has been synthesised with a quarter-car SAVGS in [3], [4] for ride comfort enhancement and the μ -synthesis approach has been proposed in [9] for a full car SAVGS to improve suspension performance. A μ -synthesis control solution has also been proposed for a full car with another recently introduced mechatronic suspension, the Parallel Active Link Suspension (PALS) [10]. Despite these achievements, the physical constraints, such as actuator torque and actuator speed constraints, are not explicitly taken into account in the previous control design. Instead by tuning associated weights in the control design it is hoped that the actuator will operate not too close to its limits. Furthermore, the previous robust control schemes

Z. Feng (zilin.feng17@imperial.ac.uk), S. A. Evangelou (s.evangelou@imperial.ac.uk) and I. M. Jaimoukha (i.jaimoukha@imperial.ac.uk) are with the Dept. of Electrical and Electronic Engineering at Imperial College London, UK.

A. Georgiou (georg611@umn.edu) is with the Dept. of Mechanical Engineering at University of Minnesota, USA.

M. Yu (m.yu14@imperial.ac.uk) and D. Dini (d.dini@imperial.ac.uk) are with the Dept. of Mechanical Engineering at Imperial College London, UK.

do not allow for continuously adapting the control solution, instead they design offline control gains that remain fixed with time. Therefore, both of these shortcomings could lead to constraint violation and performance conservativeness. In addition, in previously developed control techniques [4], [9] it is only possible to account for the road inputs as unbounded exogenous disturbances and model miss-match as structured uncertainties, which could lead to a lack of robustness in the presence of disturbances and model uncertainties with more precise characteristics.

A very promising control approach that has gained a lot of attention in the last two decades is Model Predictive Control (MPC). MPC refers to a class of algorithms in which the current control action is computed by solving online, at each sampling instant, an optimization problem based on an explicit model of the system [11]–[13]. This model-based control technique has been widely implemented in industry due to its ability to directly handle any physical and/or design constraints within its formulation [14]. An implementation of a standard MPC approach on an active suspension control application has been presented in [15]–[18]. Although it partially addresses some of the problems mentioned earlier (i.e. it does take into account constraints and updates the control gain online), it is not the preferred control method for a real-life implementation since it still lacks the potential to take into account model miss-match in the form of structured feedback uncertainties and/or external disturbances into the optimization problem. An explicit MPC formulation is presented in [19], where the OCP is designed for an ideal linear quarter-car active suspension system (known and fixed spring and damping coefficients) with a preview of road disturbances. A quadratic programming formulation of a model predictive controller based on a differential flatness derivation of the nonlinear active suspension system of a quarter car is presented in [20].

The robust formulation of MPC schemes has been the subject of extensive research with many schemes in the literature (see, for example, [21]–[28] and the reference therein). The adaptive tube-based model predictive control is presented in [29] for a vehicle active suspension system, which guarantees robustness against model uncertainties and external disturbances. Tube-based MPC methods involve initially forecasting a nominal system trajectory and ensuring that every projected closed-loop state trajectory of the uncertain system remains within a "tube" around the nominal trajectory [27], [30]–[33]. One of the major advantages of tube-based MPC is that its online computational complexity is similar to the nominal MPC formulation. However, the control performance of this method is compromised due to a fixed control gain used offline to calculate the volume of tubes based on the non-trivial concept of invariant sets. An alternative RMPC formulation using LMIs has been proposed in [23], [24], [26], [34], which does not involve any offline calculation, and therefore it is less conservative, while external disturbances and model uncertainties are considered.

In this paper, an LMI-based RMPC formulation, inspired by the algorithm proposed in [34], [35] is employed, considering a proposed uncertain linear equivalent suspension model to control a high-fidelity SAVGS quarter car system. The LMI-

based RMPC is expected to have the following advantages: i) the constraints for the actuator limits can be explicitly taken into account in the formulation of the MPC scheme, ii) the state-feedback gain and control perturbation are computed online at each sampling interval to solve the optimization problem, iii) the road inputs can be considered as exogenous disturbances with pre-defined realistic bounds against which the RMPC scheme is developed, and iv) the model uncertainty can be considered in a structured feedback manner. Therefore, the first two advantages can contribute to reduced conservativeness and improved performance in comparison to other control methods, while the last two advantages can guarantee robustness under the worst-case scenario. In addition to the RMPC controller, in this work a PI controller is also employed in parallel to the linear equivalent (and nonlinear) quarter car model, to achieve zero steady-state tracking error on the linearization point (see Section IV for more details).

In more detail, the main contributions of this paper are: i) the development of the uncertain system to capture the model mismatch between the linear equivalent model and nonlinear high fidelity model of the quarter car SAVGS, ii) the development of a coupling control strategy, which combines a RMPC scheme with PI controller to improve suspension performance while guaranteeing the robustness and stability of the quarter car SAVGS under model uncertainties and external road disturbances, and iii) numerical simulations with a nonlinear multi-body model of the SAVGS quarter car to assess the effectiveness and robustness of the proposed control scheme, as compared to the passive suspension and the actively controlled SAVGS by state-of-the-art H_∞ control.

The rest of the paper is structured as follows: Section II illustrates the nonlinear and linearised quarter-car models and describes how the uncertainties are employed in these models. Section III designs a robust control scheme with bounded disturbances and structured feedback uncertainties taken into consideration. Section IV combines the RMPC scheme detailed in section III with a PI controller to develop the overall scheme to improve suspension performance. Section V performs numerical simulations to compare the developed scheme to the passive suspension and the previously developed H_∞ control scheme for the SAVGS, with ride comfort and road holding being the primary indexes. Finally, concluding remarks are discussed in Section VI.

A. Notation

\mathbb{R} denotes the set of real numbers, \mathbb{R}^n denotes the space of n -dimensional real (column) vector. $\mathbb{R}^{n \times m}$ denotes the space of $n \times m$ real matrices and \mathbb{D}^n denotes the space of diagonal matrices in $\mathbb{R}^{n \times n}$. $\mathcal{H}(A) := A + A^T$ for $A \in \mathbb{R}^{n \times n}$ and A^T denotes the transpose of A . If $\mathbf{V} \subseteq \mathbb{R}^{p \times q}$ is a subspace, then $\mathcal{B}\mathbf{V} = \{V \in \mathbf{V} : VV^T \preceq 1\}$ denotes the unit ball of \mathbf{V} .

II. SUSPENSION MODEL AND DESIGN REQUIREMENTS

This section summarises a high-fidelity nonlinear multi-body quarter car model developed in [4] that will be applied for nonlinear simulations and evaluation. Then the nominal linear equivalent model of the quarter car model is briefly

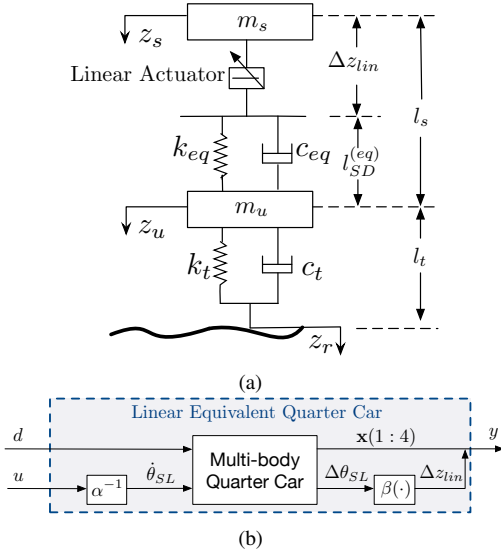


Fig. 2. (a) Schematic of SAVGS linear equivalent quarter car model (z_s and z_u are the linear equivalent displacements of the sprung and unsprung mass in the vertical direction, respectively, z_r is the vertical displacement of road surface, and $l_{SD}^{(eq)}$ is the equivalent spring-damper length); (b) transformation between linear equivalent and multi-body models of the SAVGS quarter car [4]. The function α converts the control input $u = \dot{z}_{lin}$ to the rotary single-link velocity ($\omega_{SL} = \dot{\theta}_{SL}$), and the function β converts the SL angle $\Delta\theta_{SL}$ to the linear actuator displacement Δz_{lin} . d is the derivative of the road displacement profile and is considered an exogenous unbounded disturbance, and y represents the measurable system's state $x(t) = [\dot{z}_s, \dot{z}_u, \Delta l_s, \Delta l_t, \Delta z_{lin}]^T$.

described. The nominal linear equivalent model is initially presented in [3], [4] and proved to be sufficiently accurate for developing a nominal controller, which can then be effectively utilized for controlling the vehicle's SAVGS suspension. As mentioned in Section I, the main two drawbacks of considering the nominal linear equivalent model for control design are the lack of robustness guarantees under uncertainties and the introduction of conservativeness in the control performance. To close the gap between the nonlinear and the nominal linear quarter car model, an uncertain linear equivalent model subject to parameter variation and external disturbances is derived to capture the nonlinear dynamics of the actual system.

A. Nonlinear multi-body model of quarter car SAVGS

The nonlinear multi-body quarter car model of the SAVGS-retrofitted suspension has been defined in Autosim [36], [37], which extends the conventional quarter car to include a double-wishbone geometric arrangement and a nonlinear damper force characteristic, as shown in Fig. 1 [3], [4]. It involves a sprung mass that is allowed to move vertically and an unsprung mass that is connected to it via a massless double wishbone kinematic linkage. A road tire compression force F_{tz} proportional to the tire deflection, acts on the unsprung mass to support the overall mass of the quarter car and to introduce the road forcing. The main components of a nonlinear SAVGS model consisting of the SL and its PMSM actuator and gearbox are further integrated in series with the conventional spring-damper to complete the SAVGS retrofit in the quarter car model.

B. Quarter Car SAVGS linear equivalent model (nominal)

To enable the linear robust control synthesis, a linear equivalent model of the SAVGS quarter car derived in [3], [4], as shown in Fig. 2(a), is summarized here. The equivalent model is hand-derived utilizing energy-based linearization of the quarter-car SAVGS multi-body model described in Section II-A, by also removing the main geometric nonlinearity associated with the SL rotation, as shown in Fig. 2(b). The suspension geometric nonlinearity associated with the SL angle variation ($\Delta\theta_{SL}$) is lumped into the functions α and β such that the linear equivalent model continues to be accurate for a large range of operating conditions in $\Delta\theta_{SL}$ (α and β are precisely defined later in section IV). The equations of motion of the quarter car SAVGS linear equivalent model are:

$$\begin{aligned} m_s \ddot{z}_s &= k_{eq}(\Delta l_s - \Delta z_{lin}) + c_{eq}(\dot{l}_s - \dot{z}_{lin}) \\ m_u \ddot{z}_u &= -k_{eq}(\Delta l_s - \Delta z_{lin}) - c_{eq}(\dot{l}_s - \dot{z}_{lin}) + k_t \Delta l_t + c_t \dot{l}_t. \end{aligned} \quad (1)$$

which can be written in state space form as follows:

$$\dot{x}(t) = Ax(t) + B\bar{u}(t), \quad (2)$$

where the system state is $x(t) = [\dot{z}_s, \dot{z}_u, \Delta l_s, \Delta l_t, \Delta z_{lin}]^T$, in which: a) \dot{z}_s is the sprung mass vertical velocity, b) \dot{z}_u is the unsprung mass vertical velocity, c) Δl_s is the increment of the suspension deflection $l_s = z_u - z_s$ from its nominal equilibrium state (with SL at the $\Delta\theta_{SL} = 90^\circ$ position), d) Δl_t is the increment of the tire deflection $l_t = z_r - z_u$ from its nominal equilibrium state (with SL at the $\Delta\theta_{SL} = 90^\circ$ position) and where z_s, z_u, z_r are the displacements of sprung mass, unsprung mass and road, respectively, and e) Δz_{lin} is the displacement increment of the linear actuator with respect to its nominal equilibrium state (with SL at the $\Delta\theta_{SL} = 90^\circ$ position). The system input vector is $\bar{u}(t) = [d, u]^T$, where $d = \dot{z}_r$ is the derivative of the road displacement profile taken as an exogenous unbounded disturbance, and $u = \dot{z}_{lin}$, which is the control input, is the derivative of the linear equivalent actuator displacement increment (Δz_{lin}) (see Fig. 2(a)).

The matrices in (2) are

$$A = \begin{bmatrix} -\frac{c_{eq}}{m_s} & \frac{c_{eq}}{m_s} & \frac{k_{eq}}{m_s} & 0 & -\frac{k_{eq}}{m_s} \\ \frac{c_{eq}}{m_u} & -\frac{c_{eq}+c_t}{m_u} & \frac{k_{eq}}{m_u} & \frac{k_t}{m_u} & \frac{k_{eq}}{m_u} \\ -1 & 1 & 0 & 0 & 0 \\ 0 & -1 & 0 & 0 & 0 \\ 0 & 0 & 0 & 0 & 0 \end{bmatrix}, \quad B = \begin{bmatrix} -\frac{c_{eq}}{m_s} & 0 \\ \frac{c_{eq}}{m_u} & \frac{c_t}{m_u} \\ 0 & 0 \\ 0 & 1 \\ 1 & 0 \end{bmatrix} \quad (3)$$

where m_s and m_u are the sprung and unsprung masses respectively, k_{eq} and c_{eq} are the equivalent suspension stiffness and damping coefficients (from the passive spring-damper), respectively, and k_t and c_t are the tire stiffness and damping coefficients, respectively.

C. Quarter Car SAVGS linear equivalent uncertain model

Nonlinearities and unmodeled dynamics of the actual suspension system can be approximately captured by utilizing an uncertain linearized model, which provides a more reliable basis for designing a robust controller [9]. Therefore, this work aims to close the gap between the nonlinear system and its equivalent linear version presented in Section II-B.

The first step for doing so is to consider the signal d as a bounded road disturbance signal with defined bounds that will be considered in the control design to preserve robustness, instead of an exogenous unbounded signal. It is assumed that the road profile has symmetric upper and lower bounds, with $d \in [-\bar{d}, \bar{d}]$ where \bar{d} is a positive number representing the largest road profile amplitude (see more details about \bar{d} later in subsection V). Then, it is reasonable to consider the suspension damping coefficient c_{eq} as a (time-invariant) uncertain parameter to capture its nonlinear characteristic within its operating speed range; see damper manufacturer datasheets and [10] for damper nonlinear characteristic. Its variation from the nominal (low-damper-speed) value can be captured by introducing the time-invariant norm-bounded structured uncertainty operator Δ and the uncertain input and output signals $p(t)$ and $q(t)$, respectively. Therefore, the new SAVGS quarter car model subject to additive disturbances and structured feedback uncertainties can be described as follows:

$$\begin{aligned} \dot{x}(t) &= Ax(t) + B_u u(t) + B_p p(t) + B_d d(t), \\ q(t) &= C_q x(t) + D_{qu} u(t), \\ p(t) &= \Delta q(t). \end{aligned} \quad (4)$$

The matrices in (4) are:

$$\begin{aligned} A &= \begin{bmatrix} -\frac{c_{eq}^{(nom)}}{m_s} & \frac{c_{eq}^{(nom)}}{m_s} & \frac{k_{eq}}{m_s} & 0 & -\frac{k_{eq}}{m_s} \\ \frac{c_{eq}^{(nom)}}{m_u} & -\frac{c_{eq}^{(nom)}}{m_u} + c_t & -\frac{k_{eq}}{m_u} & \frac{k_t}{m_u} & \frac{k_{eq}}{m_u} \\ -1 & 1 & 0 & 0 & 0 \\ 0 & -1 & 0 & 0 & 0 \\ 0 & 0 & 0 & 0 & 0 \end{bmatrix}, \\ B_u^T &= \left[-\frac{c_{eq}^{(nom)}}{m_s} \quad \frac{c_{eq}^{(nom)}}{m_u} \quad 0 \quad 0 \quad 1 \right], \\ B_d^T &= \left[0 \quad \frac{c_t}{m_u} \quad 0 \quad 1 \quad 0 \right], \quad B_p^T = \left[\frac{1}{m_s} \quad -\frac{1}{m_u} \quad 0 \quad 0 \quad 0 \right], \\ C_q &= \left[-c_{eq}^{(dev)} \quad c_{eq}^{(dev)} \quad 0 \quad 0 \quad 0 \right], \quad D_{qu} = \left[-c_{eq}^{(dev)} \right], \end{aligned} \quad (5)$$

in which $c_{eq}^{(nom)}$ and $c_{eq}^{(dev)}$ ($c_{eq}^{(dev)} > 0$) denote the nominal value and the maximum deviation of suspension damping coefficient c_{eq} , respectively, where:

$$c_{eq} = c_{eq}^{(nom)} \pm c_{eq}^{(dev)}. \quad (6)$$

Taking into account the operational damper speed range, it is assumed that c_{eq} can be within a $\pm 10\%$ range of its nominal value, therefore, $c_{eq}^{(dev)} = 0.1 c_{eq}^{(nom)}$. The uncertainty operator has the form $\Delta := \{\Delta \in \mathbb{R} : \Delta^T \Delta \leq 1\}$ and the disturbance set is bounded $\mathcal{D} := \{d \in \mathbb{R} : -\bar{d} \leq d \leq \bar{d}\}$.

Since the robust control design presented subsequently in Section III is developed using a discrete-time model, the continuous-time model in (4) is discretized using a zero-order hold method, where the discrete model is defined as:

$$\begin{aligned} x_{k+1} &= Ax_k + B_u u_k + B_p p_k + B_d d_k, \\ q_k &= C_q x_k + D_{qu} u_k, \\ p_k &= \Delta_k q_k. \end{aligned} \quad (7)$$

Remark 1. Note that the distribution matrices A, B_u, B_p , and so on, in (7) are the discretized versions of those in (4) and the same notation is used for simplicity.

Remark 2. In general the norm-bounded structured uncertainty operator Δ can be a time-varying parameter and can be represented as Δ_k . In the present work, it is assumed that the operator is time-invariant, thus $\Delta_k = \Delta$ for all k .

D. Objectives and constraints requirements

In this study, ride comfort and road holding are selected as the two main control objectives in suspension design [38]–[40]. As it is common in the context of the quarter-car, these two aspects of suspension performance are addressed by minimizing the vertical body acceleration of the sprung mass, \ddot{z}_s , and the vertical tire deflection, Δl_t [5]. Due to structural limitations and the physical capabilities of the actuator, three hard constraints are also used in this work for the single-link angle $\Delta \theta_{SL}$, the single-link angular velocity $\omega_{SL} = \dot{\theta}_{SL}$ (which is the control input in the nonlinear multibody quarter-car model), and the actuator single link torque T_{SL} (see Section IV-C for more details on the constraint association), respectively. Therefore, to achieve acceptable performance, the weighted quadratic values of the vertical body acceleration and the tire deflection are minimized, with the values of θ_{SL} , ω_{SL} and T_{SL} satisfying their expected bounds.

III. ROBUST MODEL PREDICTIVE CONTROL DESIGN

This section summarizes the RMPC theoretical technique in [34], which is utilized in the proposed causal state-feedback RMPC methodology for the SAVGS quarter car control problem. The general form of a system description which includes control dynamics, constraints, and cost signal is first provided. Then the algebraic formulation of an online and an offline controller, which are applied to steer a system to an admissible reference signal is explained. Considering a causal state feedback control law, the optimization problem aims to compute a state-feedback gain and a control perturbation by solving linear matrix inequalities, where the computational burden is substantially reduced without adversely affecting the tracking performance. An offline strategy to guarantee feasibility of the RMPC problem is also employed. Finally, the overall RMPC algorithm utilized in this paper is presented to summarize the control strategy that is followed in the proposed methodology.

A. System Description

Following the representation described in Section II-C, the general form of the linear discrete-time system, subject to bounded disturbances and norm-bounded structured uncertainty is illustrated as [23]:

$$\begin{aligned} \begin{bmatrix} x_{k+1} \\ q_k \\ f_k \\ z_k \end{bmatrix} &= \begin{matrix} n & n_u & n_p & n_d \\ n_q & n_f & n_z \end{matrix} \begin{bmatrix} A & B_u & B_p & B_d \\ C_q & D_{qu} & 0 & 0 \\ C_f & D_{fu} & D_{fp} & D_{fd} \\ C_z & D_{zu} & D_{zp} & D_{zd} \end{bmatrix} \begin{bmatrix} x_k \\ u_k \\ p_k \\ d_k \end{bmatrix}, \quad p_k = \Delta_k q_k, \\ \begin{bmatrix} q_N \\ f_N \\ z_N \end{bmatrix} &= \begin{bmatrix} \hat{C}_q & 0 \\ \hat{C}_f & \hat{D}_{fp} \\ \hat{C}_z & \hat{D}_{zp} \end{bmatrix} \begin{bmatrix} x_N \\ p_N \end{bmatrix}, \quad p_N = \Delta_N q_N, \end{aligned} \quad (8)$$

where $x_k \in \mathbb{R}^n$, $u_k \in \mathbb{R}^{n_u}$, $d_k \in \mathbb{R}^{n_d}$, $f_k \in \mathbb{R}^{n_f}$, $z_k \in \mathbb{R}^{n_z}$, $p_k \in \mathbb{R}^{n_p}$ and $q_k \in \mathbb{R}^{n_q}$ are the state, input, disturbance, constraint, cost,

and input and output uncertainty vectors, respectively, with $k \in \mathcal{N} := \{0, 1, \dots, N-1\}$, where N is the horizon length. In this study, it is assumed that all the states are measurable and the description includes terminal cost signal and state constraints to ensure closed-loop stability [12]. $\Delta_k \in \mathcal{B}\mathbf{\Delta}$ where $\mathbf{\Delta} \subset \mathbb{R}^{n_p \times n_q}$ is a subspace that captures the uncertainty structure. Finally, the disturbance d_k is assumed to belong to the set $\mathcal{D}_k = \{d_k \in \mathbb{R}^{n_d} : -\bar{d}_k \leq d_k \leq \bar{d}_k\}$, where the disturbance's upper bound is $\bar{d}_k > 0$ and assumed known or approximated by the application specification (see Section V for example).

Remark 3. The constrain signal f_k and the cost signal z_k are design signals linearly associated with the state and the input signal of the linear equivalent model and are used at the RMPC formulation, as will be presented in Sections III-B, IV and V.

B. Problem formulation

Given the initial state x_0 , the design of the robust model predictive controller for all $k \in \mathcal{N}$ leads to the problem of finding a feedback law u_k over the horizon N such that the cost function

$$J = \max_{d_k, \Delta_k \in \mathcal{B}\mathbf{\Delta}} \sum_{k=0}^N (z_k - \bar{z}_k)^T (z_k - \bar{z}_k), \quad (9)$$

is minimised, while the future predicted outputs satisfy the constraints $f_k \leq \bar{f}_k$ and $f_N \leq \bar{f}_N$ for all $d_k \in \mathcal{D}_k$ and all $\Delta_k \in \mathcal{B}\mathbf{\Delta}$ and for all $k \in N$. The parameter \bar{z}_k defines the reference trajectory and \bar{f}_k and \bar{f}_N are chosen to include polytopic constraints on input, state and output signals, and terminal signals respectively.

To simplify the presentation, the disturbance is re-parameterised as uncertainty by redefining $\mathcal{D}_k := \{\Delta_k^d \bar{d}_k : \Delta_k^d \in \mathcal{B}\mathbf{\Delta}^d\}$, where $\mathbf{\Delta}^d = \mathbb{D}^{n_d}$ and,

$$B_p := [B_p \ B_d], C_q := \begin{bmatrix} C_q \\ 0 \end{bmatrix}, D_{qu} := \begin{bmatrix} D_{qu} \\ 0 \end{bmatrix}, \bar{d}_k := \begin{bmatrix} 0 \\ \bar{d}_k \end{bmatrix}, p_k := \begin{bmatrix} p_k \\ d_k \end{bmatrix},$$

$$q_k := C_q x_k + D_{qu} u_k + \bar{d}_k \text{ and } n_p := n_p + n_d, n_q := n_q + n_d.$$

By defining the stacked vectors,

$$\mathbf{u} = \begin{bmatrix} u_0 \\ \vdots \\ u_{N-1} \end{bmatrix} \in \mathbb{R}^{N n_u}, \mathbf{x} = \begin{bmatrix} x_1 \\ \vdots \\ x_N \end{bmatrix} \in \mathbb{R}^{N n_n}, \boldsymbol{\zeta} = \begin{bmatrix} \zeta_0 \\ \vdots \\ \zeta_N \end{bmatrix} \in \mathbb{R}^{N n_\zeta},$$

where $\boldsymbol{\zeta}$ stands for $\mathbf{f}, \bar{\mathbf{f}}, \mathbf{p}, \mathbf{q}, \mathbf{z}, \bar{\mathbf{z}}$ or $\bar{\mathbf{d}}$ and $N_n = N n$, $N_u = N n_u$ and $N_\zeta = (N+1) n_\zeta$, we get

$$\begin{bmatrix} \mathbf{x} \\ \mathbf{q} \\ \mathbf{f} \\ \mathbf{z} \end{bmatrix} = \begin{matrix} n & N_u & N_p & 1 \\ N_n & \mathbf{A} & \mathbf{B}_u & \mathbf{B}_p & 0 \\ N_q & \mathbf{C}_q & \mathbf{D}_{qu} & \mathbf{D}_{qp} & \bar{\mathbf{d}} \\ N_f & \mathbf{C}_f & \mathbf{D}_{fu} & \mathbf{D}_{fp} & 0 \\ N_z & \mathbf{C}_z & \mathbf{D}_{zu} & \mathbf{D}_{zp} & 0 \end{matrix} \begin{bmatrix} x_0 \\ \mathbf{u} \\ \mathbf{p} \\ 1 \end{bmatrix}, \quad \mathbf{p} = \hat{\Delta} \mathbf{q}, \quad (10)$$

with $\hat{\Delta} \in \mathcal{B}\hat{\mathbf{\Delta}} \subset \mathbb{R}^{N_p \times N_q}$ where,

$$\hat{\mathbf{\Delta}} = \{\text{diag}(\Delta_0, \Delta_0^d, \dots, \Delta_{N-1}, \Delta_{N-1}^d, \Delta_N) : \Delta_k \in \mathbf{\Delta}, \Delta_k^d \in \mathbf{\Delta}^d\},$$

and where the stacked matrices in (10) (shown in bold) have the indicated dimensions and are readily obtained from iterating the dynamics in (8).

The input signal u_i is considered as a causal state feedback that depends only on states x_0, \dots, x_i (see e.g. [41]). Thus

$$\mathbf{u} = K_0 x_0 + K \mathbf{x} + \mathbf{v}, \quad (11)$$

where $\mathbf{v} \in \mathbb{R}^{N n_u}$ is the (stacked) control perturbation vector and K_0, K are the current and predicted future state feedback gains. Causality is preserved by restricting $[K_0 \ K] \in \mathcal{K} \subset \mathbb{R}^{N n_u \times N n}$, where \mathcal{K} is lower block diagonal with $n_u \times n$ blocks.

Using the definition of \mathbf{x} in equation (10) the control law in (11) can be rewritten as:

$$\mathbf{u} = \hat{K}_0 x_0 + \hat{K} \mathbf{B}_p \mathbf{p} + \hat{\mathbf{v}}, \quad (12)$$

where

$$[\hat{K}_0 \ \hat{K} \ \hat{\mathbf{v}}] = (I - K \mathbf{B}_u)^{-1} [K_0 + K \mathbf{A} \ K \ \mathbf{v}]. \quad (13)$$

Note that $(I - K \mathbf{B}_u)$ is invertible due to the lower-triangular structure and that \mathbf{u} is affine in \hat{K}_0, \hat{K} and $\hat{\mathbf{v}}$ which have the same structure as K_0, K and \mathbf{v} . A standard feedback re-parameterization gives

$$[K_0 \ K \ \mathbf{v}] = (I + \hat{K} \mathbf{B}_u)^{-1} [\hat{K}_0 - \hat{K} \mathbf{A} \ \hat{K} \ \hat{\mathbf{v}}], \quad (14)$$

and therefore $[\hat{K}_0 \ \hat{K} \ \hat{\mathbf{v}}]$ will be used as the decision variables instead. Using (12) to eliminate \mathbf{u} from (10) and re-arranging x_0 gives

$$\begin{bmatrix} \mathbf{q} \\ \mathbf{f} \\ \mathbf{z} - \bar{\mathbf{z}} \end{bmatrix} = \begin{bmatrix} \mathbf{D}_{qp} & \mathbf{D}_q^{\hat{K}_0, \hat{\mathbf{v}}} \\ \mathbf{D}_{fp} & \mathbf{D}_f^{\hat{K}_0, \hat{\mathbf{v}}} \\ \mathbf{D}_{zp} & \mathbf{D}_z^{\hat{K}_0, \hat{\mathbf{v}}} \end{bmatrix} \begin{bmatrix} \mathbf{p} \\ 1 \end{bmatrix},$$

$$:= \begin{bmatrix} \mathbf{D}_{qp} + \mathbf{D}_{qu} \hat{K} \mathbf{B}_p & \mathbf{D}_{qu} \hat{\mathbf{v}} + (\mathbf{C}_q + \mathbf{D}_{qu} \hat{K}_0) x_0 + \bar{\mathbf{d}} \\ \mathbf{D}_{fp} + \mathbf{D}_{fu} \hat{K} \mathbf{B}_p & \mathbf{D}_{fu} \hat{\mathbf{v}} + (\mathbf{C}_f + \mathbf{D}_{fu} \hat{K}_0) x_0 \\ \mathbf{D}_{zp} + \mathbf{D}_{zu} \hat{K} \mathbf{B}_p & \mathbf{D}_{zu} \hat{\mathbf{v}} + (\mathbf{C}_z + \mathbf{D}_{zu} \hat{K}_0) x_0 - \bar{\mathbf{z}} \end{bmatrix} \begin{bmatrix} \mathbf{p} \\ 1 \end{bmatrix}. \quad (15)$$

Note that all the coefficient matrices in (15) are affine in \hat{K}_0, \hat{K} and $\hat{\mathbf{v}}$. Finally, eliminating \mathbf{p} using $\mathbf{p} = \hat{\Delta} \mathbf{q}$ we get

$$\begin{bmatrix} \mathbf{f} \\ \mathbf{z} - \bar{\mathbf{z}} \end{bmatrix} = \begin{bmatrix} \mathbf{D}_f^{\hat{K}_0, \hat{\mathbf{v}}} + \mathbf{D}_{fp}^{\hat{K}} \hat{\Delta} (I - \mathbf{D}_{qp}^{\hat{K}} \hat{\Delta})^{-1} \mathbf{D}_q^{\hat{K}_0, \hat{\mathbf{v}}} \\ \mathbf{D}_z^{\hat{K}_0, \hat{\mathbf{v}}} + \mathbf{D}_{zp}^{\hat{K}} \hat{\Delta} (I - \mathbf{D}_{qp}^{\hat{K}} \hat{\Delta})^{-1} \mathbf{D}_q^{\hat{K}_0, \hat{\mathbf{v}}} \end{bmatrix}. \quad (16)$$

For convenience, constraint and cost signals can be written as $\mathbf{f} = \mathcal{F}(\hat{K}_0, \hat{K}, \hat{\mathbf{v}}, \hat{\Delta})$ and $(\mathbf{z} - \bar{\mathbf{z}})^T (\mathbf{z} - \bar{\mathbf{z}}) = \mathcal{Z}(\hat{K}_0, \hat{K}, \hat{\mathbf{v}}, \hat{\Delta})$ to emphasise dependence on the variables. By following the procedure presented by [42], the RMPC problem can be transformed to a min-max problem [21], where the objective is to find a feasible triple $(\hat{K}_0, \hat{K}, \hat{\mathbf{v}})$ that solves

$$\mathbf{J} = \min_{(\hat{K}_0, \hat{K}, \hat{\mathbf{v}}) \in \mathcal{U}} \max_{\hat{\Delta} \in \mathcal{B}\hat{\mathbf{\Delta}}} \mathcal{Z}(\hat{K}_0, \hat{K}, \hat{\mathbf{v}}, \hat{\Delta}), \quad (17)$$

The set \mathcal{U} is defined as shown in [34] to be the set of all feasible control variables $(\hat{K}_0, \hat{K}, \hat{\mathbf{v}})$ such that all the problem constraints are satisfied:

$$\mathcal{U} := \{([\hat{K}_0 \ \hat{K}], \hat{\mathbf{v}}) \in \mathcal{K} \times \mathbb{R}^{N n_u} : \mathcal{F}(\hat{K}_0, \hat{K}, \hat{\mathbf{v}}, \hat{\Delta}) \leq \bar{\mathbf{f}}, \forall \hat{\Delta} \in \mathcal{B}\hat{\mathbf{\Delta}}\}. \quad (18)$$

Since the optimization in (17) is nonconvex, the semidefinite relaxation procedure presented in [42, Lemma 1], is used by introducing an upper bound on the cost function (17), defined by γ^2 . After some matrix manipulations the inequal-

ities $\mathcal{L}(\hat{K}_0, \hat{K}, \hat{v}, \hat{\Delta}) \leq \gamma^2$ and $\mathcal{F}(\hat{K}_0, \hat{K}, \hat{v}, \hat{\Delta}) \leq \bar{\mathbf{f}}$ holds for all $\hat{\Delta} \in \hat{\mathcal{B}}\hat{\Delta}$ if there exists a solution to the nonlinear matrix inequalities [34]:

$$T_1 + \mathcal{H}(T_2 \hat{K} \mathbf{B}_p T_3) \succ 0, \quad (19)$$

$$T_1^i + \mathcal{H}(T_2^i \hat{K} \mathbf{B}_p T_3^i) \succ 0, \quad i = 1, \dots, N_f, \quad (20)$$

where

$$\begin{bmatrix} T_1 & T_2 \\ T_3 & 0 \end{bmatrix} = \begin{array}{c|ccc|c} N_z & 1 & N_q & N_p & N_u \\ \hline I & \mathbf{D}_z^{\hat{K}_0, \hat{v}} & \mathbf{D}_{zp} G^T & \mathbf{D}_{zp} S & \mathbf{D}_{zu} \\ * & \gamma^2 & (\mathbf{D}_q^{\hat{K}_0, \hat{v}})^T & 0 & 0 \\ N_q & * & R + \mathcal{H}(\mathbf{D}_{qp} G^T) & \mathbf{D}_{qp} S & \mathbf{D}_{qu} \\ N_p & * & * & S & 0 \\ \hline N_p & 0 & G^T & S & 0 \end{array},$$

$$\begin{bmatrix} T_1^i & T_2^i \\ T_3^i & 0 \end{bmatrix} = \begin{array}{c|ccc|c} 1 & N_q & N_p & N_u \\ \hline e_i^T (\bar{\mathbf{f}} - \mathbf{D}_f^{\hat{K}_0, \hat{v}}) & (\mathbf{D}_q^{\hat{K}_0, \hat{v}})^T - \frac{e_i^T}{2} \mathbf{D}_{fp} G_i^T & -\frac{e_i^T}{2} \mathbf{D}_{fp} S_i & -\frac{e_i^T}{2} \mathbf{D}_{fu} \\ N_q & * & R_i + \mathcal{H}(\mathbf{D}_{qp} G_i^T) & \mathbf{D}_{qp} S_i & \mathbf{D}_{qu} \\ N_p & * & * & S_i & 0 \\ \hline N_p & 0 & G_i^T & S_i & 0 \end{array},$$

where $([\hat{K}_0 \ \hat{K}], \hat{v}) \in \mathcal{X} \times \mathbb{R}^{N_u}$ and $(S, R, G), (S_i, R_i, G_i) \in \hat{\Psi}$ are slack variables, where $\hat{\Psi}$ is defined as:

$$\hat{\Psi} = \{(S, R, G) : S, R \succ 0, S\Delta = \Delta R, \mathcal{H}(\Delta G) = 0 \forall \Delta \in \hat{\Delta}\}. \quad (21)$$

It follows that the relaxed RMPC problem can be summarised as:

$$\min\{\gamma^2 : ([\hat{K}_0 \ \hat{K}], \hat{v}) \in \mathcal{X} \times \mathbb{R}^{N_u}, (19), (20) \text{ are satisfied}, (S, R, G), (S_i, R_i, G_i) \in \hat{\Psi}, i \in \mathcal{N}_f\}. \quad (22)$$

In this study, instead of solving multiple nonlinear matrix inequalities for the constraints as presented in (20) (one for each of the N_f constraints), a single nonlinear inequality is defined for all constraints, similarly to [34]. By doing so a reduction in the computational complexity and algorithm scalability can be achieved. Therefore without loss of generality, the multiple nonlinear inequalities presented in (20) can be written as a single nonlinear inequality as shown below:

$$\tilde{T}_1 + \mathcal{H}(\tilde{T}_2 \hat{K} \mathbf{B}_p \tilde{T}_3) \succ 0, \quad (23)$$

where $\begin{bmatrix} \tilde{T}_1 & \tilde{T}_2 \\ \tilde{T}_3 & 0 \end{bmatrix} =$

$$\begin{array}{c|ccc|c} 1 & N_f & N_q & N_p & N_u \\ \hline 2\mu (\bar{\mathbf{f}} - \mathbf{D}_f^{\hat{K}_0, \hat{v}} - M e - e\mu)^T & (\mathbf{D}_q^{\hat{K}_0, \hat{v}})^T & 0 & 0 & 0 \\ N_f & * & -\mathbf{D}_{fp} \tilde{G}^T & -\mathbf{D}_{fp} \tilde{S} & -\mathbf{D}_{fu} \\ N_q & * & \tilde{R} + \mathcal{H}(\mathbf{D}_{qp} \tilde{G}^T) & \mathbf{D}_{qp} \tilde{S} & \mathbf{D}_{qu} \\ N_p & * & * & \tilde{S} & 0 \\ \hline N_p & 0 & \tilde{G}^T & \tilde{S} & 0 \end{array},$$

and $(\tilde{S}, \tilde{R}, \tilde{G}) \in \hat{\Psi}$, $\mu \in \mathbb{R}$ and $M \in \mathbb{D}^{N_f}$ are additional slack variables. It follows that the relaxed RMPC problem can be summarised as:

$$\min\{\gamma^2 : ([\hat{K}_0 \ \hat{K}], \hat{v}) \in \mathcal{X} \times \mathbb{R}^{N_u}, (19), (23) \text{ are satisfied}, (S, R, G), (\tilde{S}, \tilde{R}, \tilde{G}) \in \hat{\Psi}\}. \quad (24)$$

The non-linearities appear in (19), (23) due to terms of the form $\hat{K} \mathbf{B}_p \Phi^T$ where Φ stands for S, G, \tilde{S} and \tilde{G} . By introducing three new slack variables Y, \tilde{Y} and X and using the Elimination lemma derived in [34], the problem can be linearised into two LMIs described below in (25) and (26):

$$\begin{bmatrix} T_1 + \mathcal{H}(T_2 \bar{K} Y^*) & * \\ (\mathbf{B}_p T_3 - \bar{K}^T T_2^T) - X Y^* & X + X^T \end{bmatrix} \succ 0 \quad (25)$$

$$\begin{bmatrix} \tilde{T}_1 + \mathcal{H}(\tilde{T}_2 \bar{K} \tilde{Y}^*) & * \\ (\mathbf{B}_p \tilde{T}_3 - \bar{K}^T \tilde{T}_2^T) - X \tilde{Y}^* & X + X^T \end{bmatrix} \succ 0, \quad (26)$$

for any $Y^* \in \mathbb{R}^{N_n \times (N_z + 1 + N_q + N_p)}$, $\tilde{Y}^* \in \mathbb{R}^{N_n \times (1 + N_f + N_q + N_p)}$ and where $\bar{K} := \hat{K} X \in \mathcal{X}$ and let $Y^* = \mathbf{B}_p T_3 (S^*, G^*) + (T_2 \hat{K}^*)^T$ and $\tilde{Y}^* = \mathbf{B}_p \tilde{T}_3 (\tilde{S}^*, \tilde{G}^*) + (\tilde{T}_2 \hat{K}^*)^T$. Then (25) and (26) are feasible. The proposed LMI-based RMPC scheme does not restrict the structure of the slack variables (R, S, G) beyond the requirements of $\hat{\Psi}$, and the reformulation of a single inequality for the constraint signal does not add any additional conservativeness into the problem; see [34] for more details.

The above formulation shows that the initial non-convex and non-linear RMPC problem can be written as an LMI optimization problem [43]. K_0, K and \mathbf{v} can be computed online and applied in the usual receding horizon MPC manner, where the first input of the control sequence \mathbf{u} is applied to the plant, the time window is shifted by 1 sampling instance, the current state is read and the process is repeated.

In this study, a lookup table is built offline to map all the initial state $x_0 \in \mathcal{X}$ to the corresponding Y^* and \tilde{Y}^* . Then the offline calculation is implemented to update the initial guesses of $\tilde{S}^*, \tilde{G}^*, \hat{K}^*$ once, after which the initial feasible solutions $Y^*(S^*, G^*, \hat{K}^*)$ and $\tilde{Y}^*(\tilde{S}^*, \tilde{G}^*, \hat{K}^*)$ are obtained and fed online (for more details refer to [34]).

By following the description that is given for both offline and online controllers, the RMPC strategy that is employed in this paper is summarized in Algorithm 1:

Algorithm 1: RMPC controller strategy

Offline calculation:

1. Build the lookup table to map all the initial states $x_0 \in \mathcal{X}$ to the corresponding Y^* and \tilde{Y}^* .
2. Compute the initial feasible solutions Y^* and \tilde{Y}^* , by reading the lookup table given the first initial state x_0 , and fix the value of Y^* and \tilde{Y}^* for the subsequent online calculation

Online calculation:

1. Read the current state x_k and set it as initial state x_0 . Then based on x_0 , extract the value of Y^* and \tilde{Y}^* from the offline calculation.
 2. Compute the triple (K_0, K, \mathbf{v}) through the two LMI procedures outlined in (25) and (26) and apply the first input of the control sequence shown in (11).
 3. Return to step 1.
-

IV. OVERALL CONTROL SCHEME DESIGN

In this section, the issues encountered when adapting the RMPC synthesized in Section III to the nonlinear multi-body

model of quarter car SAVGS introduced in Section II-A are fully discussed and the overall control scheme is designed.

A. PI control to solve the single link drifting

At low or zero road disturbance frequencies it is desired for the SL angle (Δz_{lin} in the linear equivalent model) to return to the nominal equilibrium state of $\Delta\theta_{SL} = 90^\circ$ ($\Delta z_{lin} = 0$ in the linear equivalent model), for example, after traveling over a nonzero road profile and returning to a flat road. However, due to the integrator dynamics between the control input and actuator displacement and the associated drift, this may not occur in the linear equivalent model presented in subsection III-B unless Δz_{lin} is explicitly controlled at low or zero frequencies, while a similar argument holds for the nonlinear high fidelity model. In previous work [4] developing SAVGS H_∞ control, the transfer function filtering the control output \dot{z}_{lin} has a free integrator that aims to ensure a zero steady-state tracking error of Δz_{lin} . In the present work, to avoid overcomplicating the RMPC scheme, a more conventional approach is utilized for the low frequency control, where a proportional-integral (PI) controller is introduced in parallel to the uncertain system developed in subsection II-C to ensure zero steady-state error of Δz_{lin} . As shown in Fig. 3, the exogenous reference signal of the equivalent linear actuator displacement $\Delta z_{lin}^{(ref)} = 0$ is introduced representing the nominal equilibrium of $\Delta\theta_{SL} = 90$, and its tracking error ($\Delta z_{lin}^{(trk)} := \Delta z_{lin}^{(ref)} - \Delta z_{lin}$, where $\Delta z_{lin} = rx$ with $r = [0 \ 0 \ 0 \ 0 \ 1]$ and x the state) is fed back into the PI controller of the form:

$$\dot{z}_{lin}^{(PI)} = K_p \Delta z_{lin}^{(trk)} + K_i \int \Delta z_{lin}^{(trk)} dt. \quad (27)$$

The parameters K_p and K_i can be tuned based on trial and error. Therefore, the augmented system combines the uncertain system (4) and the PI control (27), which, in continuous-time, can be described as follows:

$$\dot{\tilde{x}}(t) = \tilde{A}\tilde{x}(t) + \tilde{B}_u u(t) + \tilde{B}_p p(t) + \tilde{B}_d d(t), \quad (28)$$

where $\tilde{x}(t) = [x(t)^T \int (0 - \Delta z_{lin}) dt]^T$ is the augmented state and where

$$\tilde{A} = \begin{bmatrix} A + B_u K_p r & B_u K_i \\ r & 0 \end{bmatrix}, \quad \tilde{B}_u = \begin{bmatrix} B_u \\ 0 \end{bmatrix}, \quad (29)$$

$$\tilde{B}_d = \begin{bmatrix} B_d \\ 0 \end{bmatrix}, \quad \tilde{B}_p = \begin{bmatrix} B_p \\ 0 \end{bmatrix},$$

in which the matrices A , B_u , B_d , B_p , are defined in (5). Then the model after discretisation using a zero-order hold method is defined as:

$$x_{k+1} = \tilde{A}x_k + \tilde{B}_u u_k + \tilde{B}_p p_k + \tilde{B}_d d_k, \quad (30)$$

Remark 4. Note that the distribution matrices \tilde{A} , \tilde{B}_u , \tilde{B}_p , \tilde{B}_d , and so on, in (30) are the discretized version of those in (28) and the same notation is used for simplicity.

B. Design of cost signal

As explained in Subsection II-D, to reduce the vertical body acceleration \ddot{z}_s (ride comfort), and vertical tire deflection Δl_t (road holding), along with minimizing the input command \dot{z}_{lin}

(actuator energy consumption), the cost signal in (8) is defined as:

$$z_k = [w_1 \ddot{z}_s, w_2 \Delta l_t, w_3 \dot{z}_{lin}]^T \\ = C_z x_k + D_{zu} u_k + D_{zp} p_k + D_{zd} d_k, \quad (31)$$

with the reference cost in (9) given by $\bar{z}_k = [0 \ 0 \ 0]^T$, where w_1, w_2 and w_3 are tuneable weights to enhance performance (see Section V). Rewriting z_k in state space form the coefficient matrices are defined as follows:

$$C_z = \begin{bmatrix} -\frac{c_{eq}}{m_s} w_1 & \frac{c_{eq}}{m_s} w_1 & \frac{k_{eq}}{m_s} w_1 & 0 & -\frac{k_{eq}}{m_s} w_1 \\ 0 & 0 & 0 & w_2 & 0 \\ 0 & 0 & 0 & 0 & 0 \end{bmatrix}, \quad (32)$$

$$D_{zu} = \begin{bmatrix} -\frac{c_{eq}}{m_s} w_1 \\ 0 \\ w_3 \end{bmatrix}.$$

For $k = N$ only the terminal state x_N is predicted, thus the terminal cost signal is defined as follows:

$$z_N = [w_4 \ddot{z}_s, w_5 \Delta l_t]^T \\ = \hat{C}_z x_N + \hat{D}_{zp} p_N, \quad (33)$$

where again w_4 and w_5 are predefined weights. The coefficient matrix \hat{C}_z is defined as follows:

$$\hat{C}_z = \begin{bmatrix} -\frac{c_{eq}}{m_s} w_4 & \frac{c_{eq}}{m_s} w_4 & \frac{k_{eq}}{m_s} w_4 & 0 & -\frac{k_{eq}}{m_s} w_4 \\ 0 & 0 & 0 & w_5 & 0 \end{bmatrix}. \quad (34)$$

Since the uncertainties and additive disturbances are allowed only in state dynamics, D_{zp} , D_{zd} and \hat{D}_{zp} are zero matrices with appropriate dimensions. The dimension of the cost signal does not change but the coefficient matrices change due to augmentation of the PI controller. The cost signal is thereby redefined for the augmented system as follows:

$$\tilde{z}_k = \tilde{C}_z \tilde{x}_k + \tilde{D}_{zu} u_k, \quad (35)$$

$$\tilde{z}_N = \tilde{C}_{zN} \tilde{x}_N$$

where $\tilde{C}_z = [C_z \ 0]$, $\tilde{C}_{zN} = [\hat{C}_z \ 0]$ and $\tilde{D}_{zu} = D_{zu}$.

The robust model predictive control detailed in Section III is synthesized given the derived augmented system in (30) to achieve the (higher frequency) suspension performance objectives, as captured by (35), whilst guaranteeing the (low frequency) tracking property of Δz_{lin} .

C. Constraint conversion between nonlinear high fidelity model and linear equivalent model

The nonlinear high fidelity model built in Section II-D includes various constraints in the single-link operation, arising from packaging and actuator/gearbox constraints, involving the variables of the single-link angle $\Delta\theta_{SL}$, the single-link velocity ω_{SL} , actuator single link torque T_{SL} , PMSM power P , and so on; for more details see [5]. Since the RMPC is synthesized with the linear equivalent model, the constraints in the nonlinear model should be converted and captured by the linear model also. From the involved variables of the nonlinear model, $\Delta\theta_{SL}$ and ω_{SL} , which are constrained between their minimum and maximum values, $\Delta\theta_{SL}^{(min)}$ and $\Delta\theta_{SL}^{(max)}$, and $\omega_{SL}^{(min)}$ and $\omega_{SL}^{(max)}$, respectively, are quantified directly

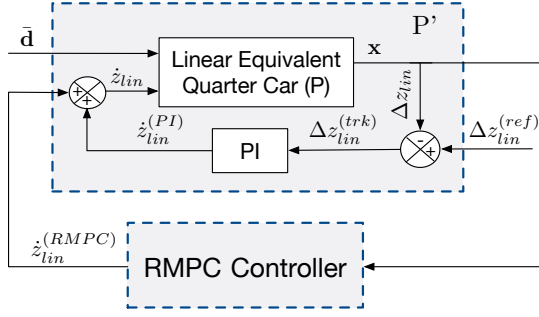


Fig. 3. RMPC scheme with PI incorporated plant model of linear equivalent quarter car SAVGS, where \bar{d} corresponds to the stacked vector for disturbance bound, P' to the new uncertain system with parallel PI incorporated, and $\Delta z_{lin}^{(ref)}$ to the exogenous reference signal of linear actuator displacement.

in the linear equivalent model via two conversion functions, respectively. Thus, function α ($= \dot{z}_{lin}/\omega_{SL}$), which has been introduced in Section II, can be approximated by a parabolic function with respect to the single-link angle ($\Delta\theta_{SL}$) [4], as shown in Fig. 4-top, and is used to convert the nonlinear variable ω_{SL} to its linear equivalent \dot{z}_{lin} . Moreover, function β ($= \Delta z_{lin}$), which is the integral of α with respect to the single-link angle ($\Delta\theta_{SL}$) [4], as shown in Fig. 4-bottom, is employed to convert the nonlinear variable $\Delta\theta_{SL}$ to its linear equivalent Δz_{lin} .

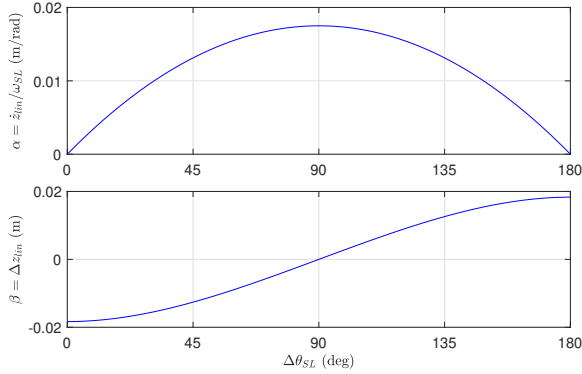


Fig. 4. Plots of functions α (top) and β (bottom) for conversion between the multibody and linear equivalent models.

The single link torque T_{SL} in the nonlinear model is constrained between $T_{SL}^{(min)}$ and $T_{SL}^{(max)}$, to avoid gearbox backlash effects and to respect the motor continuous torque limit, respectively. Function α is employed again to convert the nonlinear variable T_{SL} to its linear equivalent actuator force F_{lin} ($\alpha = T_{SL}/F_{lin}$ also) [5], where F_{lin} can be calculated by adding the equilibrium (the sprung mass weight) and increment (shown on the right hand side of the first equation in (1)) values of the equivalent passive spring force, with the equivalent damper force neglected due to its much smaller magnitude than the equivalent spring force (as verified by simulations). Thus, F_{lin} can be expressed in terms of the states Δl_s and Δz_{lin} , as follows:

$$F_{lin} = m_s g + k_{eq}(\Delta l_s - \Delta z_{lin}). \quad (36)$$

Hence, the constraint signal in (8), capturing all the constraints that are possible to consider in the control synthesis, is defined as:

$$f_k = [\Delta z_{lin}, -\Delta z_{lin}, \Delta l_s - \Delta z_{lin}, -\Delta l_s + \Delta z_{lin}, \dot{z}_{lin}, -\dot{z}_{lin}]^T \\ = C_f x_k + D_{fu} u_k + D_{fp} p_k + D_{fd} d_k, \quad (37)$$

where,

$$C_f = \begin{bmatrix} 0 & 0 & 0 & 0 & 1 \\ 0 & 0 & 0 & 0 & -1 \\ 0 & 0 & 1 & 0 & -1 \\ 0 & 0 & -1 & 0 & 1 \\ 0 & 0 & 0 & 0 & 0 \\ 0 & 0 & 0 & 0 & 0 \end{bmatrix}, \quad D_{fu} = \begin{bmatrix} 0 \\ 0 \\ 0 \\ 0 \\ 1 \\ -1 \end{bmatrix} \quad (38)$$

The upper bound of constraint signal f_k in (18) is defined as:

$$\bar{f}_k = \left[\beta \left(\Delta\theta_{SL}^{(max)} \right), -\beta \left(\Delta\theta_{SL}^{(min)} \right), \frac{\left(\frac{T_{SL}^{(max)}}{\alpha} - m_s g \right)}{k_{eq}}, \right. \\ \left. \frac{\left(m_s g - \frac{T_{SL}^{(min)}}{\alpha} \right)}{k_{eq}}, \alpha \omega_{SL}^{(max)}, -\alpha \omega_{SL}^{(min)} \right]^T. \quad (39)$$

For $k = N$ only the terminal state x_N is predicted, thus the terminal constraint signal is defined as follows:

$$f_N = [\Delta z_{lin}, -\Delta z_{lin}, \Delta l_s - \Delta z_{lin}, -\Delta l_s + \Delta z_{lin}]^T \\ = \hat{C}_f x_N + \hat{D}_{fp} p_N, \quad (40)$$

The upper bound of terminal constraint signal \bar{f}_N in (9) is defined as:

$$\bar{f}_N = \left[\beta \left(\Delta\theta_{SL}^{(max)} \right), -\beta \left(\Delta\theta_{SL}^{(min)} \right), \frac{\left(\frac{T_{SL}^{(max)}}{\alpha} - m_s g \right)}{k_{eq}}, \right. \\ \left. \frac{\left(m_s g - \frac{T_{SL}^{(min)}}{\alpha} \right)}{k_{eq}} \right]^T. \quad (41)$$

The matrix \hat{C}_f is defined by the first four rows of the C_f in (38). Similarly to the cost signal in (31) and (33), the D_{fp} , D_{fd} and \hat{D}_{fp} matrices are equal to zero with appropriate dimension. After augmentation of the PI controller, the dimension of constraint signal stays the same but the coefficient matrices change due to augmentation of the PI controller and thereby defined as follows:

$$\tilde{f}_k = \tilde{C}_f \tilde{x}_k + \tilde{D}_{fu} u_k \\ \tilde{f}_N = \tilde{C}_{fN} \tilde{x}_N \quad (42)$$

where $\tilde{C}_f = [C_f \ 0]$, $\tilde{C}_{fN} = [\hat{C}_f \ 0]$ and $\tilde{D}_{fu} = D_{fu}$. The upper bounds \bar{f}_k and \bar{f}_N remain the same.

It is noted that the minimum and maximum values of the PMSM electrical power P , $-P$ (power flow to the PMSM) and

\bar{P} (power flow from the PMSM), respectively,

$$-P \leq P \leq \bar{P}, \quad (43)$$

are not possible to include as constraints in the RMPC synthesis because of the nonlinearity of such constraints. Instead, they are only imposed in the actuator control model (block ‘Single-link actuator’ in Fig. 5) in the simulation of the nonlinear multibody model, via the PMSM inner (current) and outer (velocity) control loops, by saturating the dq voltage references to the DC-AC converter of the PMSM and the magnetizing q current reference to the inner control loop, respectively, as explained in Sections 4.3 and 4.4 of [5].

The block diagram in Fig. 5 shows the proposed overall closed-loop control scheme used for closed-loop simulations with the high fidelity nonlinear model.

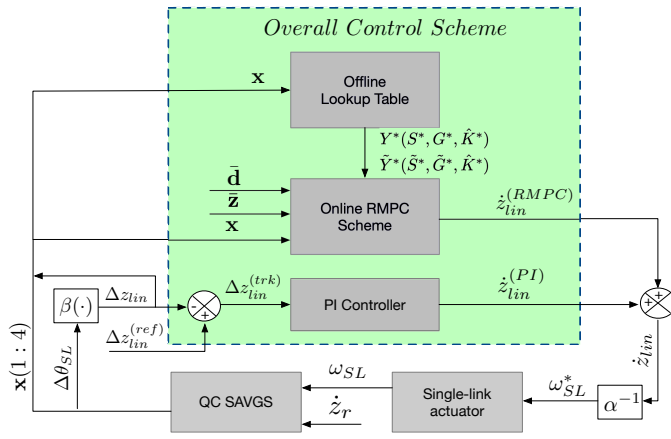


Fig. 5. Overall simulation block diagram, which contains the high fidelity nonlinear model of quarter car and actuator (‘QC SAVGS’ and ‘Single-link actuator’, respectively, where ω_{SL}^* is the reference of ω_{SL} tracked by the actuator) and the proposed coupled closed-loop control scheme. The ‘Online RMPC Scheme’ uses the linear equivalent uncertain quarter car model and initial feasible sets (Y^*, \tilde{Y}^*) based on offline created lookup tables. The first four elements of the state x as defined in the subsection II-B are measurable at the output of the high-fidelity model and the last state component (Δz_{lin}), which is also used as input to the PI controller, is computed through the function β and the measurable output $\Delta \theta_{SL}$ of the high fidelity model, as explained in subsection IV-C.

D. Benchmark H_∞ control scheme

The H_∞ control scheme designed in [4] is used as the benchmark scheme in the present work. It uses the same nominal linear equivalent model of (2) and similarly aims to minimize single link displacement tracking error at low frequencies, and vertical body acceleration and tire deflection at higher frequencies. Moreover, the zero convergence of the SL angle is addressed via a free integrator. For more details refer to [4].

V. NUMERICAL SIMULATIONS AND ANALYSIS

In this section, with the nonlinear multi-body quarter car SAVGS model described in Section II-A, and the control strategies proposed in Sections III and IV, a group of ISO driving maneuvers, containing, i) sinusoidal profile, ii) smoothed bump and hole, and iii) random road class A-C, are tested

to evaluate the performance and robustness of the overall synthesized controller, which will be denoted as the RMPC controller. The parameter values of the vehicle (corresponding to a GT car [4]), SAVGS actuator [4], [5], structured uncertainty, system constraints, disturbance bounds, reference cost, weights of the cost function, prediction horizon, and PI control gains are shown in Table I.

TABLE I
MAIN PARAMETERS OF SAVGS QUARTER CAR NONLINEAR MULTI-BODY AND LINEAR EQUIVALENT MODELS, AND RMPC AND PI CONTROL, USED IN NUMERICAL SIMULATIONS

Description	Symbol	Value
weight of sprung mass	m_s	320 kg
weight of unsprung mass	m_u	49 kg
tire’s radial stiffness	k_t	275000 N/m
tire’s radial damping	c_t	300 kg
equivalent spring stiffness	k_{eq}	59987 N/m
actuator maximum power limit	P	500 W
actuator minimum power limit	$-P$	-1500 W
nominal suspension damping	$c_{eq}^{(nom)}$	2087.4 Ns/m
suspension damping deviation	$c_{eq}^{(dev)}$	208.74 Ns/m
upper bound of SL angle	$\Delta \theta_{SL}^{(max)}$	160 deg
lower bound of SL angle	$\Delta \theta_{SL}^{(min)}$	20 deg
upper bound of continuous SL torque	$T_{SL}^{(max)}$	97 Nm
lower bound of continuous SL torque	$T_{SL}^{(min)}$	0 Nm
upper bound of SL angular velocity	$\omega_{SL}^{(max)}$	13 rad/s
lower bound of SL angular velocity	$\omega_{SL}^{(min)}$	-13 rad/s
upper bound of road disturbance	d_k	0.15 m/s
vertical body acceleration weight	w_1	$\sqrt{10}$
vertical tire deflection weight	w_2	$\sqrt{10}$
actuator energy consumption weight	w_3	$10\sqrt{6}$
vertical body acceleration terminal weight	w_4	20
vertical tire deflection terminal weight	w_5	20
prediction horizon	N	5
PI proportional gain	K_p	5
PI integral gain	K_i	1

In addition to what was done in [4], which imposed the same single-link actuator power limits of 500 W for both directions of actuator power flow, in this work $\bar{P} \leq P$ to allow for higher power flows when generating as compared to motoring.

The bound on the disturbance (\bar{d}_k), which is based on the road profile, is initially chosen as the maximum value of the vertical road velocity. However, when implementing this value in different driving manoeuvres, it is hard to achieve feasibility in the optimization problem. Therefore, the value of the disturbance bound is relaxed in this work and chosen as 0.15 m/s for all the driving manoeuvres to guarantee a feasible solution. Note that for random roads A, B and C, the vertical road velocities are within the defined range for 100%, 95.6% and 85.3% of the time, respectively. Furthermore, in the case studies presented in this section, it is found that this setting is sufficient to derive well-performing controllers that satisfy all the constraints.

Initial feasible triples $Y^*(S^*, G^*, \hat{K}^*)$ and $\tilde{Y}^*(\tilde{S}^*, \tilde{G}^*, \hat{K}^*)$ are computed offline utilizing the proposed method in [34], where the initial state x_0 is assumed to be within a bounded set \mathcal{X} which includes all the possible values that the state can take, based on the geometry and dynamics of the system.

Remark 5. Alternatively, the initial parameters $S^*, G^*, \tilde{S}^*, \tilde{G}^*$ and \hat{K}^* can be initially set to zero at $t = 0$ and then at every sampling time their values can be updated by the slack variables $(S, G, \tilde{S}, \tilde{G})$ and control value K^* computed by the online RMPC problem presented in (24). Note that this strategy does not guarantee initial feasibility of the RMPC problem, however, if the problem is solvable at $t = 0$, the upcoming optimal control problems presented in (24) have a solution.

The weights of the RMPC cost signal (w_1, w_2 and w_3) are tuned using trial and error, while the terminal cost weights (w_4 and w_5) are chosen larger than w_1 and w_2 , which enhance convergent performance and stability. To maintain the computational time of the online control problem within the discretized sampling time, the prediction horizon is set as $N = 5$. Also, the PI parameters are tuned by trial and error to achieve good tracking of the SL angle reference at low frequencies. Note that a) the tuning of the PI controller is done first, without the RMPC being in place, and b) the tuning of the RMPC weights is done with the PI controller in place and with its parameters already tuned. This is to achieve the higher frequency suspension performance requirements of ride comfort and road holding simultaneously with the low-frequency SL angle tracking requirements, but without the RMPC interfering much with the low-frequency tracking of the SL angle and vice versa.

A. Simulation With Harmonic Road

Fig. 6 presents the time response results for the body acceleration, tire deflection, suspension travel and single-link angle of the quarter-car in response to a sinusoidal road disturbance of frequency 2 Hz, for the passive, H_∞ and RMPC controllers. It can be seen that the H_∞ controller can significantly attenuate the performance objectives, with a 67% and 64% root mean square value (RMS) drop in the sprung mass acceleration and the tire deflection, respectively, as compared to the passive suspension. The RMPC controller achieves further improvements by reducing further body acceleration by 18.7% and tire deflection by 19.8%, as compared to the H_∞ controller. Moreover, Fig. 7 indicates that the RMPC control scheme utilizes a larger part of the available actuator output torque-speed operating range than the H_∞ scheme does. It does so while still satisfying all the hard (torque and speed) and soft (power) constraints of the SAVGS actuator, which also reflects on the slightly larger suspension travel and single-link angle with the RMPC than with the H_∞ scheme in Fig. 6.

B. Simulation With Smoothed Bump and Hole

Speed bumps or humps are common in some roadways and are normally approximated as a raised cosine shape. The mathematical representation of the wheel road height while running over a standard laterally uniform bump with 0.0275 m

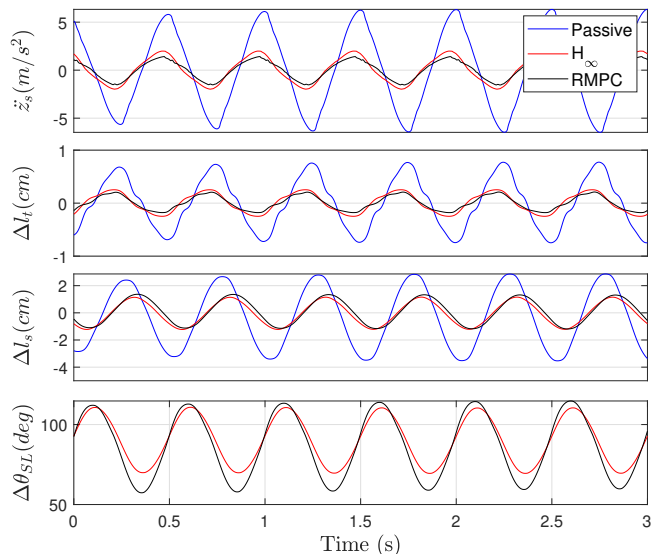


Fig. 6. Numerical simulation results with the nonlinear high fidelity model (top to bottom): the sprung mass acceleration (\ddot{z}_s), tire deflection increment (Δl_t) and suspension deflection increment (Δl_s) with respect to the initial nominal equilibrium state (SL at the $\Delta\theta_{SL} = 90^\circ$ position), and single-link angle ($\Delta\theta_{SL}$), when the quarter-car SAVGS is undergoing a harmonic road profile with 2 Hz frequency and 2.75 cm peak-to-peak amplitude, for the passive suspension, and H_∞ and RMPC active suspension control.

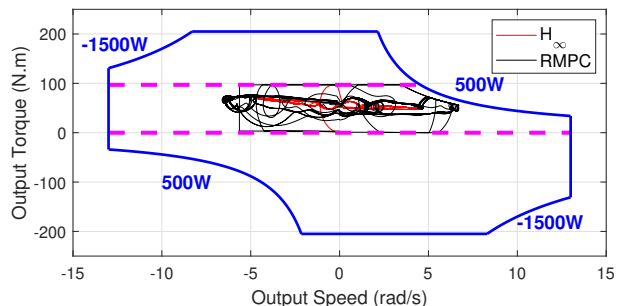


Fig. 7. SAVGS actuator output torque (T_{SL}) vs. output speed (ω_{SL}) characteristics from simulation with the nonlinear high fidelity model, when the quarter-car SAVGS is undergoing a sinusoidal road profile with 2 Hz frequency and 2.75 cm peak-to-peak amplitude, for different cases of active suspension control, with actuator peak and continuous limit boundaries shown in blue solid and magenta dashed lines, respectively.

height and 1.4 m length, and after a distance of 4.15 m a hole with 0.0275 m height and 1.4 m length, is expressed as follows:

$$h_{bh}(x) = \begin{cases} h_c(1 - \cos(\frac{2\pi x}{1.4})), & 0 < x \leq 1.4 \\ h_c(-1 + \cos(\frac{2\pi(x-5.55)}{1.4})), & 5.55 < x \leq 6.95 \\ 0, & \text{elsewhere} \end{cases} \quad (44)$$

where $h_c = 0.01375$.

Numerical simulation results at a forward speed of 10 km/h over the road profile in (44) with the passive and SAVGS-retrofitted quarter car with different active control cases, are shown in Figs. 8 and 9. Similarly to the sinusoidal road cases, the H_∞ scheme outperforms the passive suspension. In turn the RMPC outperforms the H_∞ active suspension with

a 27.68% and 25.95% further reduction in terms of sprung mass acceleration and tire deflection peak values, respectively. It can also be observed that the PI controller of the overall RMPC scheme successfully restores the single-link angle to its equilibrium value (SL at the $\Delta\theta_{SL} = 90^\circ$ position) after each of the bump and hole events. Furthermore, as it can be seen in Fig 9, the actuator constraints are satisfied by both control schemes, but the actuator output torque-speed operating range is more widely used in the RMPC scheme.

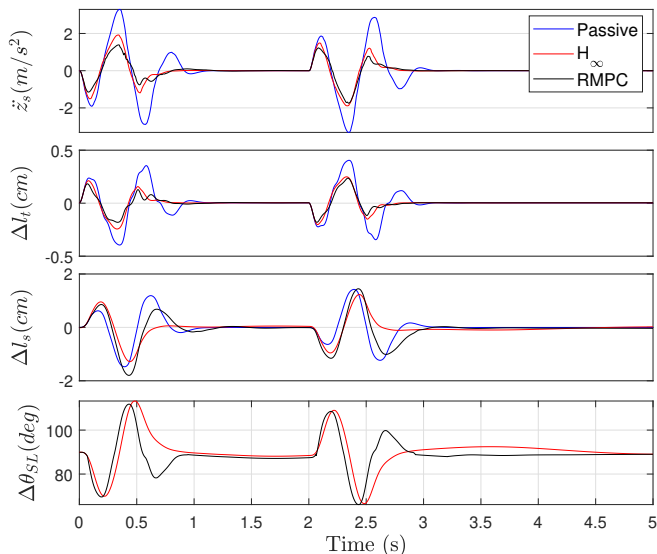


Fig. 8. Numerical simulation results with the nonlinear high fidelity model (top to bottom): the sprung mass acceleration (\ddot{z}_s), tire deflection increment (Δl_t) and suspension deflection increment (Δl_s) with respect to the initial nominal equilibrium state (SL at the $\Delta\theta_{SL} = 90^\circ$ position), and single-link angle ($\Delta\theta_{SL}$), when the quarter-car SAVGS is running at 10 km/h driving speed over a smoothed bump (0-2 s) and hole (2-4 s), both with 2.75 cm in road height and 1.4 m length (profile in (44)), for the passive suspension, and H_∞ and RMPC active suspension control.

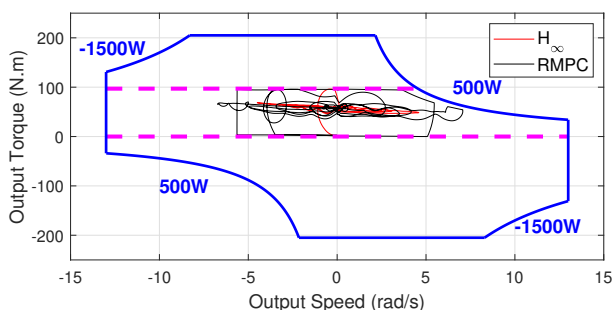


Fig. 9. SAVGS actuator output torque (T_{SL}) vs. output speed (ω_{SL}) characteristics from simulation with the nonlinear high fidelity model, when the quarter-car SAVGS is running at 10 km/h driving speed over a smoothed bump and hole road profile as in (44), for different cases of active suspension control, with actuator peak and continuous limit boundaries shown in blue solid and magenta dashed lines, respectively.

C. Simulation with Random Road

The ISO random roads are used to simulate road unevenness. The measured vertical surface data of different

road profiles, such as streets, highways as well as off-road terrain are usually described in terms of their power spectral density (PSD), which is defined in the frequency domain as follows [44]:

$$G_d(n) = 10^{-6} \cdot 2^{2k} \left(\frac{n}{n_0}\right)^{-\bar{\omega}}, \quad (45)$$

where $n \in [n_{min}, n_{max}]$ is the spatial frequency (cycles per meter), $k = 2$ to 9 corresponds to the road roughness classes A to H, respectively, $n_0 = 0.1$ cycles/m is the reference spatial frequency, and $\bar{\omega} = 2$ is a constant.

The random road profile in the time domain is obtained as the addition of a series of harmonic signals with varying amplitudes and spatial frequencies as follows [5]:

$$h_{ran}(x) = \sum_{n_i=n_{min}}^{n_{max}} A_i \cos(2\pi n_i x + \phi_i), \quad (46)$$

$$A_i = \sqrt{2 \Delta n G_d(n_i)} = 2^{(k+1/2)} 10^{-3} \sqrt{\Delta n} \left(\frac{n_0}{n_i}\right),$$

in which $h_{ran}(x)$ is the random road height. Sinusoidal components are related to the spatial frequency n_i and the random phase ϕ_i , which is distributed uniformly over the range $(0, 2\pi)$. Δn is the spatial frequency step, and A_i is the amplitude corresponding to the spatial frequency n_i (for more details refer to [5]).

The parameters of the random road profiles for simulations with the nonlinear high fidelity model are selected as follows: the spatial frequency range $[n_{min}, n_{max}] = [0.01, 10]$ cycles/m for the general on-road vehicles, the road length $L = 1$ km, $\Delta n = 0.001$ cycles/m since $\Delta n \leq 1/L$ should be satisfied, and k takes one of three values to correspond to three different cases of highway road unevenness, a good quality highway (class A, $k = 2$), an average quality road (class B, $k = 3$), and a poor quality road (class C, $k = 4$). The simulations are conducted with a forward speed of 100 km/h of the SAVGS-retrofitted quarter-car over each of the three road sections, and are used to validate the improvement of the ride comfort and road holding.

The nonlinear simulation power spectral densities (PSDs) of the sprung mass acceleration and the tire deflection over the random roads (classes A-C) are shown in Fig. 10. The H_∞ and RMPC controllers both give a notably improved performance in terms of ride comfort and road holding at around human-sensitive frequencies (1-6 Hz) as compared to the passive case. It can also be observed that the RMPC outperforms H_∞ in terms of sprung mass acceleration attenuation at almost all frequencies, and in terms of tire deflection reduction at frequencies below approximately 7 Hz. Despite this tire deflection deterioration above approximately 7 Hz with RMPC, the sprung mass acceleration and tire deflection RMS values detailed in Table II demonstrate that overall there is improvement in both metrics by RMPC as compared to both the passive and H_∞ active suspension. Thus, the RMPC reduces the sprung mass RMS acceleration by 5.6% (road C) up to 12.3% (road A) and the tire RMS deflection by 0.4% (road C) up to 7% (road A), as compared to H_∞ , with the reductions as compared to the passive suspension being even larger.

The output torque-speed operating points for the actuators

are plotted in Fig. 11 alongside the power, torque and speed constraint envelope. Out of the three different random road cases, the most power-consuming event, for the poor quality random road C, is presented. Results show that the proposed RMPC control utilizes the actuator capabilities fully: the operating torque-speed points approach the boundaries without exceeding them. The H_∞ control only employs part of the actuator capability leading to the conservative performance in terms of ride comfort and road holding, as discussed in Fig. 10.

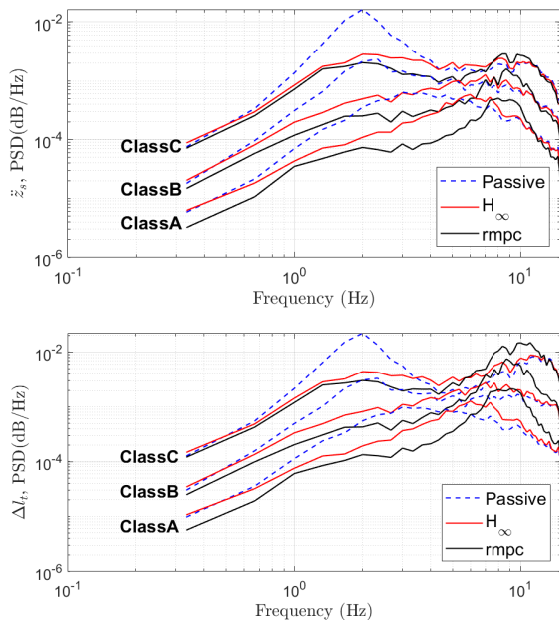


Fig. 10. Numerical simulation results: the PSD estimate of the sprung mass acceleration (top) and tire deflection (bottom), when the quarter car SAVGS is travelling with a forward speed of 100 km/h over random roads (Classes A-C) for the passive suspension and different cases of active suspension control.

TABLE II

RMS VALUES OF \ddot{z}_s AND Δl_t WITH PASSIVE SUSPENSION AND TWO DIFFERENT CONTROLLERS FOR RANDOM ROAD CLASSES A-C. COLUMNS DENOTE PASSIVE SUSPENSION, H_∞ , RMPC, AND PERCENTAGE IMPROVEMENT OF RMPC WITH RESPECT TO H_∞ (LAST COLUMN). THE NUMBERS IN THE BRACKETS DENOTE THE PERCENTAGE OF IMPROVEMENT OF THE TWO ACTIVE CONTROL METHODS WITH RESPECT TO THE PASSIVE SUSPENSION.

	Symbol	Passive	H_∞	RMPC	
C	\ddot{z}_s	1.910	1.600 (16%)	1.510 (21%)	5.6%
	Δl_t	0.281	0.270 (4.1%)	0.269 (4.5%)	0.4%
B	\ddot{z}_s	1.060	0.950 (9.3%)	0.870 (16.8%)	8.4%
	Δl_t	0.144	0.147 (-1.9%)	0.142 (2.1%)	3.4%
A	\ddot{z}_s	0.630	0.570 (8.6%)	0.500 (19.5%)	12.3%
	Δl_t	0.083	0.086 (-2.2%)	0.080 (2.5%)	7.0%

VI. CONCLUSIONS

The recently proposed mechatronic suspension of the Series Active Variable Geometry Suspension (SAVGS) [2], [3], [45] is investigated in the application to a quarter car, with suspension damping nonlinearities and road profiles taken into

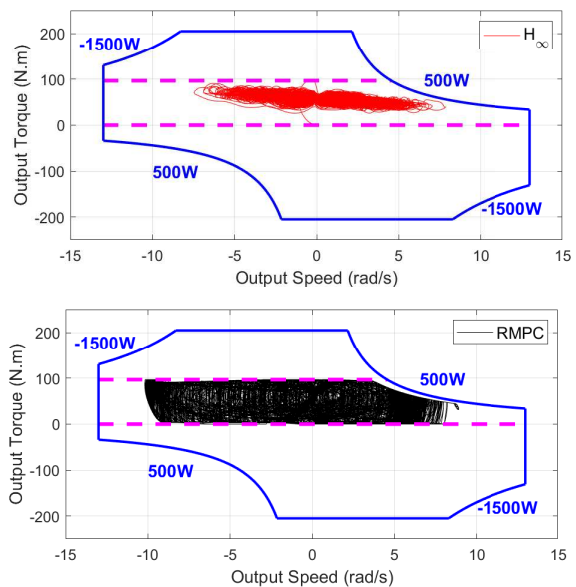


Fig. 11. SAVGS actuator output torque (T_{SL}) vs. output speed (ω_{SL}) characteristics from simulation with the nonlinear high fidelity model, when the quarter-car SAVGS is traveling with a forward speed of 100 km/h over a random road profile (class C) for H_∞ control (top) and RMPC (bottom), with actuator peak and continuous limit boundaries shown in blue solid and magenta dashed lines, respectively.

consideration in the suspension control design as uncertainties and bounded disturbances, respectively, revealing promising potential in terms of ride comfort and road holding improvement.

An LMI-based robust model predictive control (RMPC) scheme with an uncertain system description is proposed as the control design that can effectively improve the road holding and ride comfort performance at the human sensitive frequency range (1-6 Hz), as compared to the passive suspension and a benchmark H_∞ control, while system stability and constraint satisfaction are preserved. In particular, the proposed RMPC scheme provides in simulations of ISO maneuvers of sinusoidal road, smoothed bump and hole, and random road A, B and C with a high fidelity model of the quarter-car with SAVGS decent performance improvement as compared to H_∞ , with 18.7%, 19.8% and 12.3% in terms of rms body acceleration (ride comfort), respectively. Improvements over the H_∞ control in terms of tire deflection (road holding) are also provided. Overall, the results illustrate the effectiveness of the proposed control method to extract further performance out of the recently proposed SAVGS architecture, as compared to previous control methods, utilizing the SAVGS actuator at its limits of capability.

REFERENCES

- [1] R. N. Jazar, *Vehicle dynamics: theory and application*. Springer, 2017.
- [2] C. Arana, S. A. Evangelou, and D. Dini, "Series active variable geometry suspension application to chassis attitude control," *IEEE/ASME Transactions on Mechatronics*, vol. 21, no. 1, pp. 518–530, 2016.
- [3] —, "Series active variable geometry suspension application to comfort enhancement," *Control Engineering Practice*, vol. 59, pp. 111–126, 2017.

- [4] M. Yu, C. Arana, S. A. Evangelou, and D. Dini, "Quarter-car experimental study for series active variable geometry suspension," *IEEE Transactions on Control Systems Technology*, vol. 27, no. 2, pp. 743–759, 2017.
- [5] C. Arana, "Active variable geometry suspension for cars," Ph.D. dissertation, Imperial College London, 2015.
- [6] C. Cheng and S. A. Evangelou, "Series active variable geometry suspension robust control based on full-vehicle dynamics," *Journal of Dynamic Systems, Measurement, and Control*, vol. 141, no. 5, p. 051002, 2019.
- [7] M. Yu, C. Cheng, S. A. Evangelou, and D. Dini, "Robust control for a full-car prototype of series active variable geometry suspension," in *2019 IEEE 58th Conference on Decision and Control (CDC)*. IEEE, 2019, pp. 7615–7622.
- [8] —, "Series active variable geometry suspension: Full-car prototyping and road testing," *IEEE/ASME Transactions on Mechatronics*, 2021.
- [9] Z. Feng, M. Yu, C. Cheng, S. A. Evangelou, I. M. Jaimoukha, and D. Dini, "Uncertainties investigation and μ -synthesis control design for a full car with series active variable geometry suspension," *IFAC-PapersOnLine*, vol. 53, no. 2, pp. 13 882–13 889, 2020.
- [10] Z. Feng, M. Yu, S. A. Evangelou, I. M. Jaimoukha, and D. Dini, "Mu-synthesis pid control of full-car with parallel active link suspension under variable payload," *IEEE Transactions on Vehicular Technology*, vol. 72, no. 1, pp. 176–189, 2023.
- [11] D. Q. Mayne, J. B. Rawlings, C. V. Rao, and P. O.M. Scokaert, "Constrained model predictive control: Stability and optimality," *Automatica*, vol. 36, no. 6, pp. 789–814, 2000.
- [12] J. B. Rawlings and D. Q. Mayne, *Model predictive control: Theory, computation and design*. Madison, Wisconsin: Nob Hill, August 2017.
- [13] J. M. Maciejowski, *Predictive control with constraints*. Edinburgh: Pearson Education Limited, 2002.
- [14] S. J. Qin and T. A. Badgwell, "A survey of industrial model predictive control technology," *Control Engineering Practice*, vol. 11, pp. 733–764, 2003.
- [15] Mehra, Raman K and Amin, Jayesh N and Hedrick, Karl J and Osorio, Carlos and Gopalasamy, Srinivasan, "Active suspension using preview information and model predictive control," in *Proceedings of the 1997 IEEE international conference on control applications*. IEEE, 1997, pp. 860–865.
- [16] C. Göhrle, A. Schindler, A. Wagner, and O. Sawodny, "Model predictive control of semi-active and active suspension systems with available road preview," in *2013 European Control Conference (ECC)*. IEEE, 2013, pp. 1499–1504.
- [17] J. Yao, M. Wang, Z. Li, and Y. Jia, "Research on model predictive control for automobile active tilt based on active suspension," *Energies*, vol. 14, no. 3, 2021. [Online]. Available: <https://www.mdpi.com/1996-1073/14/3/671>
- [18] E. Enders, G. Burkhard, and N. Munzinger, "Analysis of the influence of suspension actuator limitations on ride comfort in passenger cars using model predictive control," *Actuators*, vol. 9, no. 3, 2020. [Online]. Available: <https://www.mdpi.com/2076-0825/9/3/77>
- [19] J. Theunissen, A. Sornioti, P. Gruber, S. Fallah, M. Ricco, M. Kvasnica, and M. Dhaens, "Regionless explicit model predictive control of active suspension systems with preview," *IEEE Transactions on Industrial Electronics*, vol. 67, no. 6, pp. 4877–4888, 2020.
- [20] D. Rodriguez-Guevara, A. Favela-Contreras, F. Beltran-Carbajal, C. Sotelo, and D. Sotelo, "A differential flatness-based model predictive control strategy for a nonlinear quarter-car active suspension system," *Mathematics*, vol. 11, no. 4, 2023. [Online]. Available: <https://www.mdpi.com/2227-7390/11/4/1067>
- [21] P. O.M. Scokaert and D. Q. Mayne, "Min-max feedback model predictive control for constrained linear system," *IEEE Transaction on Automatic Control*, no. 43, pp. 1136–1142, 1998.
- [22] E. Kerrigan and J.M. Maciejowski, "Feedback min-max model predictive control using a single linear program: robust stability and the explicit solution," *International Journal of Robust and Nonlinear Control*, vol. 14, pp. 395 – 413, 2004.
- [23] M. V. Kothare, V. Balakrishnan, and M. Morari, "Robust constrained model predictive control using linear matrix inequalities," *Automatica*, vol. 32, no. 10, pp. 1361–1379, 1996.
- [24] F. A. Cuzzola, J. C. Geromel, and M. Morari, "An improved approach for constrained robust model predictive control," *Automatica*, vol. 38, no. 7, pp. 1183–1189, 2002.
- [25] G. Emanuele and C. Alessandro, "Receding horizon control strategies for constrained lpv systems based on a class of nonlinearly parameterized lyapunov functions," *IEEE Transactions on Automatic Control*, vol. 57, no. 9, pp. 2354–2360, 2012.
- [26] F. Tahir and I. M. Jaimoukha, "Causal state-feedback parameterizations in robust model predictive control," *Automatica*, vol. 49, no. 9, pp. 2675–2682, 2013.
- [27] J. Fleming, B. Kouvaritakis, and M. Cannon, "Robust tube mpc for linear systems with multiplicative uncertainty," *IEEE Transactions on Automatic Control*, vol. 60, no. 4, pp. 1087–1092, 2014.
- [28] J. Hanema, M. Lazar, and R. Tóth, "Heterogeneously parameterized tube model predictive control for lpv systems," *Automatica*, vol. 111, p. 108622, 2020.
- [29] M. Kang, R. Chen, and Y. Li, "Adaptive tube-based model predictive control for vehicle active suspension system," in *2020 4th CAA International Conference on Vehicular Control and Intelligence (CVCI)*. IEEE, 2020, pp. 720–725.
- [30] W. Langson, I. Chrysochoos, S. V. Raković, and D.Q. Mayne, "Robust model predictive control using tubes," *Automatica*, vol. 40, no. 1, pp. 125 – 133, 2004.
- [31] D. Q. Mayne, M. Seron, and J. D. Dona, "Robust model predictive control of constrained linear systems with bounded disturbances," *Automatica*, vol. 41, no. 2, pp. 219–224, 2005.
- [32] M. Bujarbaruah, U. Rosolia, Y. R. Stürz, and F. Borrelli, "A simple robust mpc for linear systems with parametric and additive uncertainty," in *2021 American Control Conference (ACC)*. IEEE, 2021, pp. 2108–2113.
- [33] W. Vilaivannaporn, S. Boonsith, W. Pornputtipitak, and P. Bumroongsri, "Robust output feedback predictive controller with adaptive invariant tubes and observer gains," *International Journal of Dynamics and Control*, vol. 9, no. 2, pp. 755–765, 2021.
- [34] A. Georgiou, F. Tahir, I. M. Jaimoukha, and S. A. Evangelou, "Computationally efficient robust model predictive control for uncertain system using causal state-feedback parameterization," *IEEE Transactions on Automatic Control*, pp. 1–8, 2022.
- [35] A. Georgiou, "Robust model predictive control for linear systems subject to norm-bounded model uncertainties and disturbances: An implementation to industrial directional drilling system," Ph.D. dissertation, Imperial College London, 2022.
- [36] M. Sayers, "Autosim," *Vehicle System Dynamics*, vol. 22, no. S1, pp. 53–56, 1993.
- [37] C. Mousseau, M. W. Sayers, and D. Fagan, "Symbolic quasi-static and dynamic analyses of complex automobile models," *Vehicle System Dynamics*, vol. 20, no. sup1, pp. 446–459, 1992.
- [38] R. Sharp and S. Hassan, "An evaluation of passive automotive suspension systems with variable stiffness and damping parameters," *Vehicle System Dynamics*, vol. 15, no. 6, pp. 335–350, 1986.
- [39] H. E. Vongierke, "The iso standard: Guide for the evaluation of human exposure to whole-body vibration," in *NASA. Langley Res. Center The 1975 Ride Quality Symp.*, 1975.
- [40] R. Sharp and D. Crolla, "Road vehicle suspension system design-a review," *Vehicle system dynamics*, vol. 16, no. 3, pp. 167–192, 1987.
- [41] J. Skaf and . S. P. Boyd, "Design of affine controllers via convex optimization," *IEEE Transactions on Automatic Control*, vol. 55, pp. 2476–2487, 2010.
- [42] F. Tahir and I. Jaimoukha, "Causal state-feedback parameterization in robust model predictive control," *Automatica*, vol. 49, no. 9, pp. 2675–2682, 2013.
- [43] S. Boyd, L. E. Ghaoui, and V. Balakrishnan, *Linear matrix inequalities in system and control theory*. Philadelphia: SIAM, 1994.
- [44] ISO, "8608:2016, Mechanical vibration - Road surface profiles - reporting of measured data," Geneva, Switzerland, 2016.
- [45] M. Yu, S. A. Evangelou, and D. Dini, "Model identification and control for a quarter car test rig of series active variable geometry suspension," *IFAC-PapersOnLine*, vol. 50, no. 1, pp. 3376–3381, 2017.